



Using all seismic arrivals in shallow seismic investigations

Gabriel Fabien-Ouellet ^{*}, Richard Fortier

Département de géologie et de génie géologique, Université Laval, Québec, Canada



ARTICLE INFO

Article history:

Received 5 August 2013

Accepted 16 December 2013

Available online 7 January 2014

Keywords:

Seismic reflection

SV waves

Multichannel analysis of surface wave

Seismic refraction tomography

Surface wave filter

Hydrogeophysics

ABSTRACT

Near surface seismic investigations are expensive and time-consuming. Moreover, seismic processing usually focuses on one particular type of wave and wastes much of the information contained in seismic records that could be used to make near surface seismic surveys more valuable and cost effective. A workflow is proposed herein that combines seismic refraction tomography, multichannel analysis of surface waves (MASW), and seismic reflection using P-waves and SV-waves, which takes advantage of P-wave first arrivals, Rayleigh waves, and P-wave and SV-wave reflections, respectively. The use of the proposed methodology is shown through three case studies carried out in the Outaouais region, Quebec, Canada, using a 24-channel seismograph, vertical geophones, and a sledgehammer. The results show that it is possible to acquire SV-reflections at sites where a strong velocity reversal is present at the surface using only vertical geophones. Under that condition, or more generally when two component geophones are used, the proposed workflow leads to two complementary stacked sections: 1) an SV-wave section that has a high resolution even at shallow depths but can lack coherency and 2) a P-wave section that has better coherency but is blind at shallow depths. Two velocity models are also produced: an SV-wave model that combines the results from MASW and SV-wave reflections and a P-wave model that combines the results from seismic refraction and P-wave reflections. The workflow uses the frequency variant linear move-out (FV-LMO) surface wave filter, which is much more efficient than band pass or f-k filters to process SV waves. The value of many near surface seismic surveys can thus be enhanced by processing all propagation modes, especially when SV-wave reflections are present due to their high resolution.

© 2014 Elsevier B.V. All rights reserved.

1. Introduction

Seismic energy propagates in the earth through different types of waves (P, SH, SV, Rayleigh, Love, Stoneley) that can undergo reflections, refractions, conversions from one type to another and diffractions (Aki and Richards, 2002). Conventional seismic investigations focus on a particular seismic arrival. For instance, one of the most popular seismic methods to map the depth to bedrock, the seismic refraction method, uses direct and refracted P-waves (Hagedoorn, 1959; Palmer, 1981). First arrivals can also be processed using tomographic inversion techniques that require far less input from the interpreter, can take into account velocity inversions and support one-direction shot spreads (Sheenan et al. 2005; White, 1989; Zang and Toksöz, 1998). In many cases, the geophones and shot spacings used for refraction tomography are similar to those used in seismic reflection surveys, with shots at every two or three geophone intervals (Lanz et al., 1998).

Seismic reflection surveys normally use only reflections from P-waves or SH waves. Recent work by Pugin et al. (2008, 2009) showed the power of using SV-wave reflections, which exhibit high resolution at very shallow depths, similar to SH reflections. Although three component

geophones are recommended to successfully acquire SV-wave reflections in all terrain conditions, Pugin et al. (2013) found that their polarization is more vertical in soft clayey soils and horizontal when the medium is hard, such as a sand deposit or outcropping rock. This indicates that SV-wave reflections may be recorded with vertical geophones over soft soils at certain sites.

Rayleigh waves can be processed by multichannel analysis of surface waves (MASW). This method has proven to be a reliable technique to assess SV-wave velocities (Park et al., 1998; Xia et al., 2002, 2003) and, in certain cases, their quality factor (Lai et al., 2002; Xia et al., 2012). The spread configuration of the geophones and seismic shots used in a typical MASW survey is similar to common seismic reflection field geometries (Park et al., 2002b).

As it was previously mentioned, these methods use a similar geometry in the field and multiple propagation modes carrying useful information are usually generated and recorded. Moreover, the unwanted modes of propagation are often regarded as noise and much effort is spent removing them. Therefore, only a fraction of the available information in seismic gathers is used and processed. By obtaining more information out of the same dataset using a more complete signal processing approach, the seismic acquisition can become more valuable and cost efficient. A workflow is presented herein that integrates the processing techniques specific to MASW, seismic refraction tomography, P-wave seismic reflection and SV-wave seismic reflection. The objective is to obtain useful information from all the seismic arrivals.

* Corresponding author at: Département de géologie et de génie géologique, Université Laval, Québec (QC), G1V 0A6, Canada. Tel.: +1 418 656 2746.

E-mail addresses: gabriel.fabien-ouellet.1@ulaval.ca (G. Fabien-Ouellet), Richard.Fortier@ggl.ulaval.ca (R. Fortier).

The workflow puts an emphasis on SV-wave reflections due to their higher resolution than P-wave reflections.

The use of this processing workflow is illustrated through three case studies. The first case illustrates the full workflow for a survey designed for the acquisition of SV reflections. The second case describes the application of a surface wave filter, the frequency variant linear move-out (FV-LMO) filter proposed by Park et al. (2002a) which is a logical extension of the proposed workflow. The third case shows how the workflow can help identify the presence or absence of SV-wave reflections. The conditions necessary to acquire SV-wave reflections using only vertical geophones are discussed first.

2. Acquisition of SV-waves

The most common way to record S-waves is by using cross-line horizontal geophones with a cross-line polarized source (Haines and Ellefsen, 2010; Hunter et al., 2002). Using that configuration, SH-waves can be generated and recorded. In contrast, vertically polarized shear waves can be generated with any conventional sources and can be recorded by inline vertical and horizontal geophones (Helbig and Mesdag, 1982).

The direction of polarization of SV reflections depends on the angle of incidence and the velocity distribution and usually varies with offset. For that reason, vertical and horizontal geophones are usually required. However, in some geological settings, a significant amount of SV-wave energy can be recorded with vertical geophones, even at short offsets. One such setting is the presence of a strong velocity inversion close to the surface (Fig. 1). According to Snell's law, an incoming ray is horizontally shifted if a high velocity layer lies on top of a much slower layer. In that case, the particle motion becomes mostly vertical. Such a situation is quite common in clay deposits that are affected by freeze-thaw and wetting-drying cycles, which cause over-consolidation of the surficial layer that significantly increases its shear wave velocity (Motazedian and Hunter, 2008). Another common case is a paved or gravel road constructed on soft soils: the pavement then acts as a high velocity layer. In such conditions, a significant amount of SV-wave energy can be recorded using only vertical geophones as shown in Section 6. However, careful planning and testing are required to use only vertical geophones to acquire SV-waves and two-component (2-C) geophones are preferable in all circumstances.

3. Processing workflow

The processing workflow that combines MASW, seismic refraction tomography and SV- and P-wave reflection inversion is shown in Fig. 2. The SV- and P-waves are processed separately. The starting point of both processing flows is the spatially referenced seismic data. For the SV-wave processing, MASW is first performed to build an S-wave velocity model. The dispersion curves produced during this analysis are used to filter the surface waves. The SV-wave reflections are then inverted to obtain a stacked section and a combined MASW/

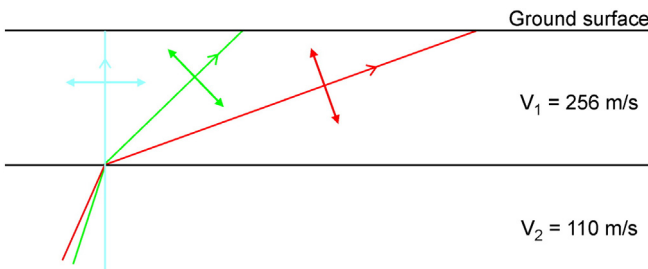


Fig. 1. Due to the presence of a strong velocity inversion close to the ground surface, the SV-waves particle motion is deflected to vertical. The velocities for this example are taken from a seismic piezocone penetration test (SCPTu) performed along the survey line of case study 1 (Fig. 3b) (Fabien-Ouellet et al., 2014).

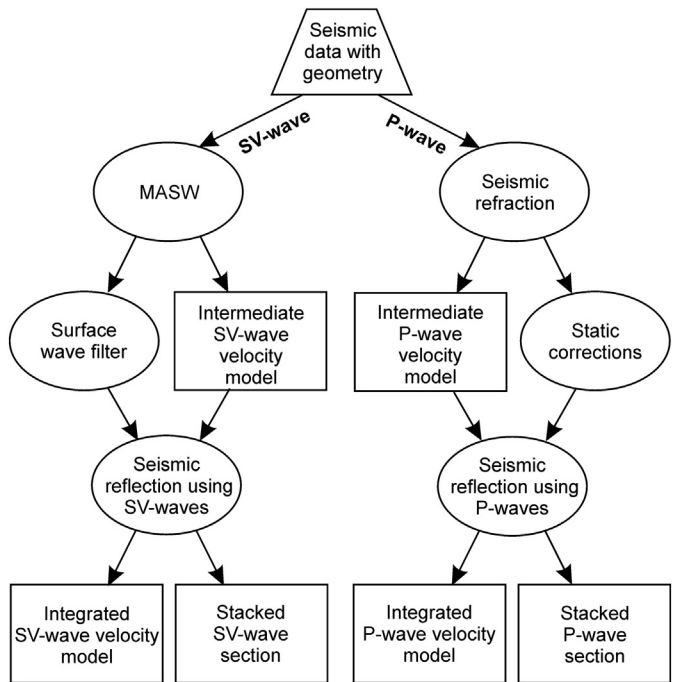


Fig. 2. Processing workflow combining MASW, SV-wave reflections, seismic refraction tomography, and P-wave reflections.

reflection velocity model. The P-wave processing begins by picking first breaks, which are used for seismic refraction tomography and for surface static corrections. The P-wave reflections are then processed using the tomographic velocity model as a first estimate for the stacking velocities. Similar to the SV-wave processing, a P-wave stacked section and a combined refraction/reflection velocity model are produced. This is a general methodology, and the specific procedures of each inversion method could vary. The details of the present study are given in Section 6.

Even though 2-C geophones were not used in any of the case studies presented herein, this methodology is particularly well-suited for 2-C processing because all four seismic arrivals should be present in those records. In contrast, SV-wave reflection processing must be skipped for sites where SV-waves cannot be observed in the vertical component, but the rest of the workflow is still valid because surface waves and P-waves should usually be present.

4. The frequency variant linear move-out filter

It is critical to remove Rayleigh waves before performing the CMP inversion of the SV reflections. The velocities of P-waves and Rayleigh waves are so different that most of the surface wave energy is removed by CMP stacking. However, because Rayleigh waves travel at approximately 90% of the velocity of SV-waves, surface waves often overlap and even hide SV reflections. For this reason, performing the CMP inversion of SV reflections without previously removing surface waves can lead to spurious reflections on the stacked section.

Surface waves are normally removed using band-pass filters, f-k filters or muting. However, the frequency spectrums of surface waves and SV-waves often overlap and band-pass filters cannot effectively remove surface waves without removing a significant part of the desired signal. f-k filters are not well adapted for this filtering because the energy of surface waves is difficult to identify in the f-k domain. Moreover, the use of a simple velocity fan is problematic because of the multimodal and dispersive nature of surface waves. One of the most common techniques to remove surface waves is muting. However, muting can be subjective and a compromise must be made between removing surface waves and preserving SV reflections. It is often

impossible to remove surface waves without removing a significant part of the reflection energy, especially for very shallow reflections.

Park et al. (2002a) proposed an effective method for filtering surface waves. Their method is based on the same transformation as the MASW method. Given the observed modes of surface waves $C_i(\omega)$, the frequency variant linear move-out (FV-LMO) $\varphi(\omega, x)$ is obtained according to the following equation:

$$\varphi(\omega, x) = e^{i\omega x/C_i(\omega)}. \quad (1)$$

Given observed data $d(x, t)$, the Fourier transform $D(\omega, x)$ is calculated. The inverse FV-LMO correction is then applied:

$$D_{FV-LMO}(\omega, x) = e^{-i\omega x/C_i(\omega)} D(\omega, x). \quad (2)$$

This correction horizontally aligns each frequency of the surface waves but anything that does not share the same dispersion relation is not aligned. All of the horizontal energy is then removed using an f-k filter. To obtain the filtered data, the FV-LMO correction is applied and the inverse Fourier transform is performed. To filter all of the energy of the Rayleigh waves, the dispersion curve of each mode is identified and the FV-LMO filter is performed separately for each mode.

5. Study sites

The seismic surveys presented herein were performed in the Outaouais region, Quebec, Canada. The locations of the study sites are shown in Fig. 3. The general stratigraphy of the region consists of a thin layer of till above bedrock that is covered in places by glaciolacustrine sediments. This sequence is usually overlain by a thick glaciomarine unit that was deposited by the Champlain Sea. As shown in Fig. 3, two of the seismic lines were performed over the soft glaciomarine deposits, namely the Buckingham (Section 6.1) and the Shawville (Section 6.2) case studies. However, a glaciolacustrine sand deposit is present in the lake Green case study (Section 6.3).

The three surveys were acquired under the *Programme d'acquisition des connaissances sur les eaux souterraines en Outaouais* (PACES), which was a regional study of groundwater in the Outaouais region. One of the main objectives of the PACES project was to acquire new information for areas where existing databases failed to provide a comprehensive hydrogeological overview. To achieve this objective, seismic methods were used to spatially extend information from nearby wells (as for the Shawville case study) and to obtain the stratigraphy for sites where drilling could not be performed (as for the Buckingham and Lake Green case studies).

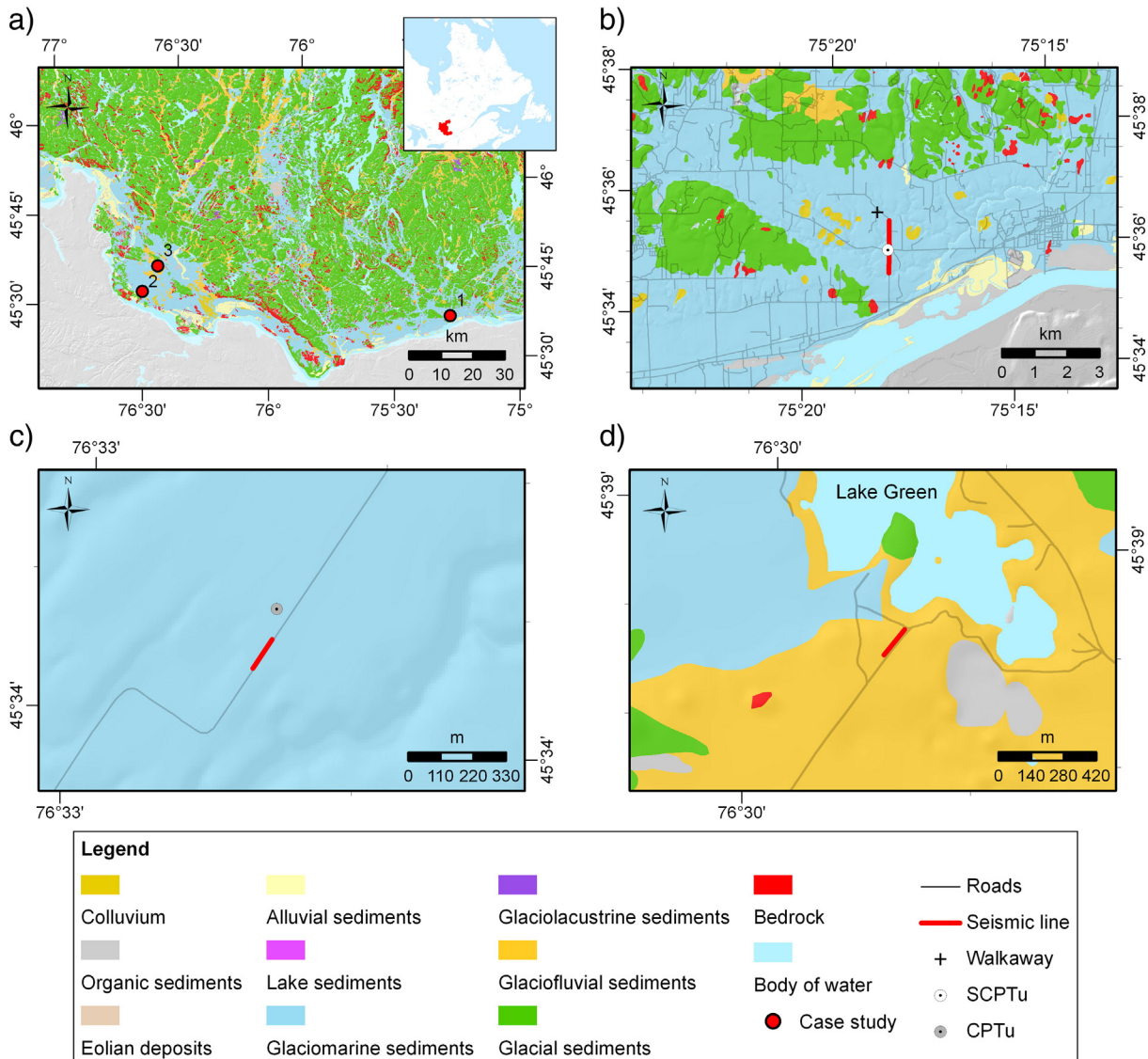


Fig. 3. Quaternary geologic maps: a) locations of the three study sites along the Ottawa River, b) Buckingham case study, c) Shawville case study, d) Lake Green case study. Modified from Hurtubise et al. (2012) and Leduc et al. (2013).

6. Case studies

6.1. Buckingham case study: application of the workflow

The goal of the seismic survey in the Buckingham case study was to characterize an aquifer that is confined by a surficial sensitive clay deposit. According to boreholes located in the survey area, a clay unit more than 30 m thick overlies a glaciofluvial sand and gravel unit, and the bedrock is 40 to more than 100 m deep. However, no wells were located directly along the line. One of the objectives of this investigation was to confirm and clarify the general stratigraphy described above.

6.1.1. Acquisition

This seismic survey was designed for the acquisition of SV- and P-wave reflections, but the configuration also allowed for the acquisition and processing of Rayleigh waves and P-wave first arrivals. The acquisition parameters described here are essentially the same for all of the surveys; any differences will be described when introducing each case study.

The seismic acquisition was performed using a 24-channel engineering seismograph (Stratavisor NZ-24) and 40-Hz vertical geophones. The impact of an 8-kg sledgehammer on a steel plate lying horizontally on the ground surface was used as a seismic source. This source was very efficient in the field and only two shots were performed and stacked for each shot point. Moreover, strong SV-waves were generated with this seismic source. Each survey line was located on the shoulder of a gravel road, which acted as the hard layer that refracts SV-waves vertically (Section 2) and facilitated the execution of the survey.

The configuration used in this hydrogeophysical investigation is similar to the SH-wave reflection surveys carried out by Guy et al. (2003) and Pugin et al. (2004). The geophones were located 0.75 m apart to avoid aliasing while the seismic shots were located every 3 m along the survey line. In the Buckingham case study, long offsets were required to reach the bedrock at a depth of 100 m, and each shot position was used four times as the geophone spreads were moved forward along the line. The configuration when the records are sorted by seismic shot location is shown in Fig. 4.

This configuration is not only adequate to process SV- and P-wave reflections, but it is also very similar to the recommendations for 2D MASW surveys for targets at depths exceeding 50 m (Park et al., 2002b). The only difference is the natural frequency of the geophones; 40 Hz geophones were used in this study, while 4.5 Hz geophones are normally recommended.

6.1.2. Presence of SV-wave reflections

Before performing an SV seismic reflection survey using vertical geophones, it is necessary to check that SV-wave reflections are indeed recorded by the vertical geophones. This can be achieved by walkaway tests (Steeple and Miller, 1998) performed at several locations along the planned seismic line. In our case, the choice of vertical over 2-C

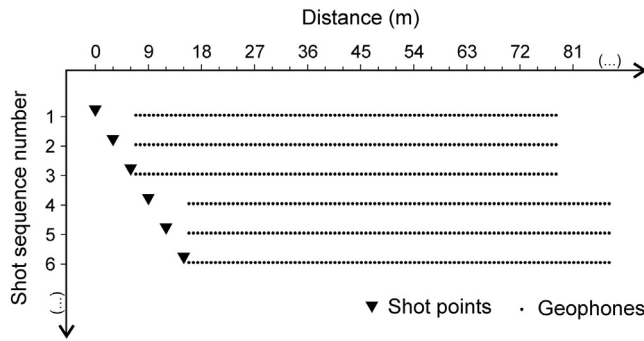


Fig. 4. Configuration of geophones and seismic shots after sorting the records relative to their seismic shot locations.

geophones was dictated by budget restrictions, but a 2-C survey would have been preferable.

An example of such a test conducted for the Buckingham case study in a farm field near the survey line is given in Fig. 5, where a coherent SV-wave reflection is clearly present at approximately 600 ms. P-wave reflections are also present at times less than 400 ms. This result was judged to be good enough to perform the seismic survey. It is worth mentioning that a PS reflection is present at 400 ms, which is indicated in Fig. 5. PS reflections can be observed on most of the records in the first two case studies. It is possible to process them, and they can provide an independent stacked section (Pugin et al., 2013). However, they were not processed in this study.

6.1.3. SV-wave processing

The first step for processing SV-waves is the MASW method. This was performed as described in Park et al. (1998, 1999). The phase-velocity transformation was performed on CMPs binned at twice the shot interval (6 m) to improve the signal-to-noise ratio at low frequencies. The fundamental mode, as well as the higher modes, was identified manually during the dispersion analysis, but only the fundamental mode was considered for the inversion. The S-wave velocities at this site were expected to vary continuously with depth (Fabien-Ouellet et al., 2014), so a 15-layer initial model reaching a maximum depth of 15 m was used for the inversion. Each dispersion curve was separately inverted until convergence, and the P-wave velocities and the thickness of each layer were kept constant. All of the curves were then smoothed horizontally with a moving median filter that was three curves wide, and they were inverted separately again until convergence. The inversion was performed with the software Seisimager/SW. Several algorithms are available for the inversion of Rayleigh waves that takes into account higher modes (Xia et al. 2000), effective dispersion curves (Lai and Rix, 1998) or that uses full waveforms (O'Neill et al., 2003). The use of these algorithms could provide better S-wave velocity models, but the inversion of the fundamental mode alone gave satisfactory results. Dispersion curves from the fundamental mode and higher modes were also used to filter the surface waves with the FV-LMO filter.

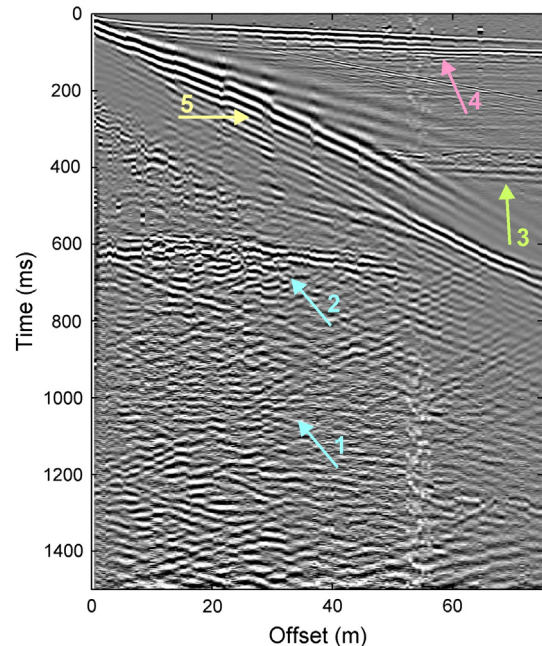


Fig. 5. A walkaway test acquired near the survey line of the Buckingham case study (see Fig. 3 for its location). The blue (nos. 1 and 2), green (no. 3) and red (no. 4) arrows indicate SV, PS and P reflections, respectively, while the yellow arrow (no.5) indicates Rayleigh waves.

Table 1

CMP processing of SV-wave reflections. The steps identified by an asterisk were performed with in-house MATLAB codes based on the CREWES algorithms.

Processing step	Description
1. Surface wave filter*	Described in Section 4
2. CMP binning	Bin length: 0.75 m
3. Bad trace removal*	Automatic based on S/N ratio
4. Scaling	AGC with a window of 1 s
5. Semblance analysis	Includes MASW model
6. NMO correction	Stretch mute: 75%
7. Alpha trim stacking	Alpha percentage: 75%
8. AGC	Window: 400 ms
9. Band-pass filter	10, 15, 125, and 250 Hz trapezoid frequencies
10. Median filter	Length: 5 traces
11. Depth conversion	Using f-k migration and the smoothed velocity model
12. Topographic shift	

The processing flow for SV-wave reflections is summarized in Table 1. The P- and S-wave processing was performed with the CREWES MATLAB package (Margrave, 2003) in combination with in-house MATLAB codes and GEDCO Vista. After filtering the surface waves, Common Middle Point gathers (CMP) were defined with a 0.75 m bin. Bad traces were then removed based on their signal-to-noise (S/N) ratios. The traces were scaled, and a semblance analysis

was performed at every 6 m using the MASW velocity model at times where there were no reflections. The traces were then corrected for the normal move-out and stacked. Depth conversion was performed by f-k migration, and the topographic correction was performed by shifting each trace to the datum level.

The SV-wave processing steps are illustrated in Fig. 6. Clear SV-wave reflections can be observed from 200 ms to the end of the gather at every offset (Fig. 6a). The reflections are more coherent than in the walkaway test shown in Fig. 5. One potential explanation is that the velocity inversion caused by the road material was stronger than that of the over-consolidated clay layer in the farm field where the walkway test was performed.

The phase-velocity transformation for the CMP gather is shown in Fig. 6b. The energy of the Rayleigh waves is separated into several modes of propagation, and each mode was considered for surface wave filtering. The fundamental mode shown in the inset in Fig. 6b was inverted to obtain the S-wave velocity model in Fig. 6c. To evaluate the errors caused by picking the fundamental mode, the higher and lower envelopes of the dispersion curves of the fundamental mode (inset in Fig. 6b) were picked and inverted (Fig. 6c). CMP gather no. 43 after application of the surface wave filter is shown in Fig. 6d. Most of the energy of the surface waves is removed. The semblance analysis, including the MASW model, and the NMO corrected gather are shown

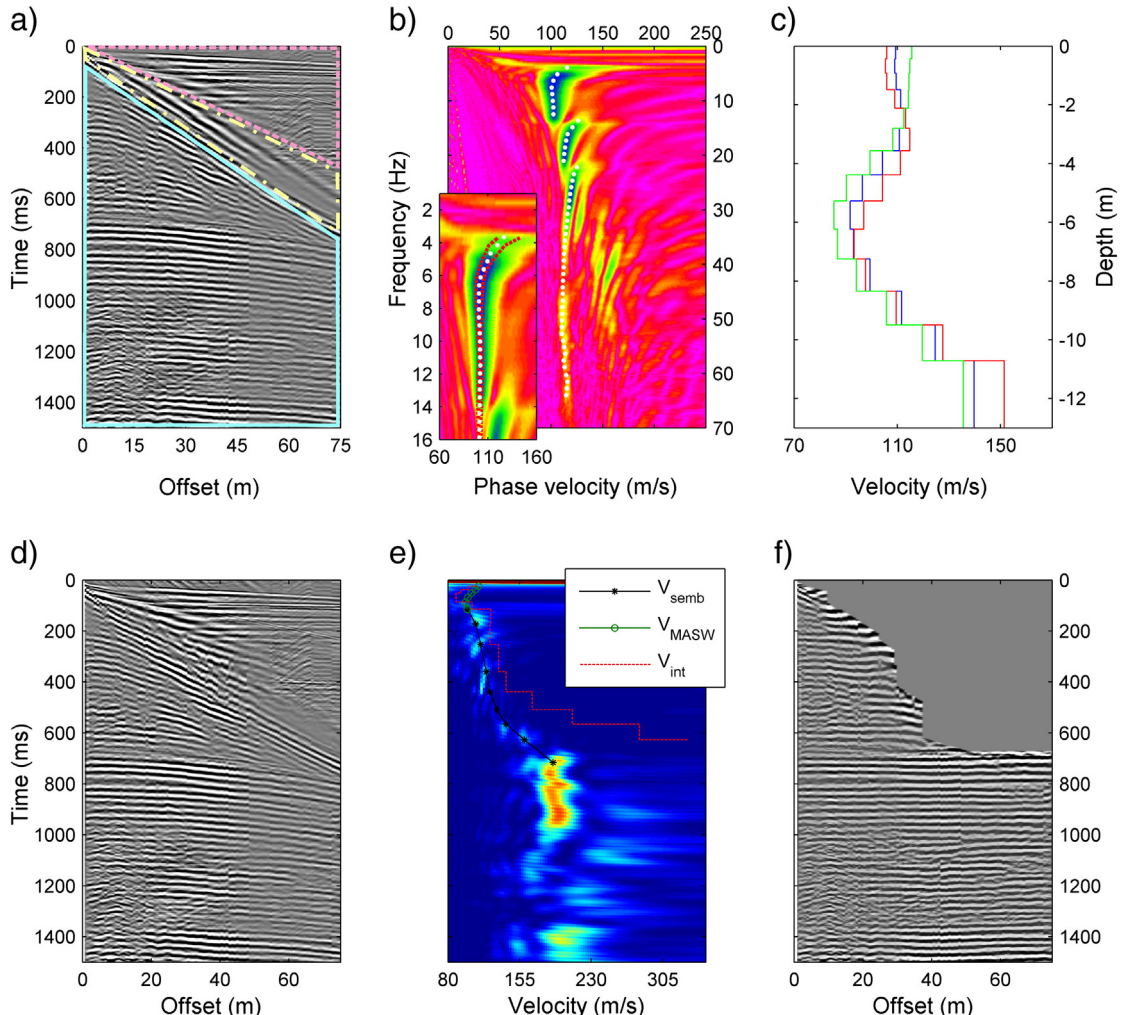


Fig. 6. An example of the SV-wave processing: a) CMP gather no. 43 along the survey line of the Buckingham case study, where SV-waves are located in the blue solid line frame, Rayleigh waves in the yellow dash-dotted line frame and P-waves in the red dashed line frame, b) dispersion curves showing the fundamental and higher modes of propagation (inset: detail of the fundamental mode; uncertainties are identified with red lines), c) SV-wave velocity model in purple obtained from the inversion of the fundamental mode (the red and green lines are the estimated errors), d) the same CMP gather after filtering of surface waves using all modes, e) semblance analysis of SV-waves using the MASW results (green dots), and f) NMO-corrected CMP gather with a stretch mute of 100%. (For interpretation of the references to color in this figure legend, the reader is referred to the web version of this article.)

in Fig. 6e and f, respectively. A more thorough discussion of the integration of MASW and SV-wave reflections can be found in Fabien-Ouellet et al. (2014). Following the muting of the samples in which the stretch in frequency exceeds 60%, a considerable amount of the energy at far offsets is muted on the NMO corrected gather. This can be problematic for this dataset and can cause some reflections to be strongly attenuated on the stacked section (see Section 6.1.5).

Because the stacking velocities of the S-waves and P-waves are very different, the stretch mute removes most of the P-wave energy on the CMP gather after the NMO correction. This, along with the fact that S-waves are much more energetic at short offsets on the CMP gathers, ensures that no P-wave energy remains on the S-wave stacked section.

6.1.4. P-wave processing

The first step for the P-wave processing is seismic refraction tomography using wavepath eikonal traveltimes (WET) inversion with the software Rayfract (Schuster and Quintus-Bosz, 1993). This algorithm supports the inversion of seismic refraction tomography with an end-on spread and one-way shots. First breaks were picked for every shot without any previous processing. The final velocity model was obtained after twenty iterations of the WET inversion algorithm.

The first breaks were also used to apply surface static corrections as described in Pugin and Pullan (2000). An average model that included three layers was assigned to the entire survey, and each trace was shifted in time to align the picked first breaks with the synthetic arrivals from the average model. Only one model was used because the P-wave velocity model obtained by seismic refraction tomography was constant along the entire survey.

The processing flow for P-wave reflections is summarized in Table 2 and is similar to the SV-wave processing. The main difference is the use of predictive deconvolution to remove multiples. Moreover, a band-pass filter was used to remove the low frequency noise shown in Fig. 7a. This enhanced lower energy reflections on the CMP gathers (Fig. 7d).

The workflow for P-wave processing is presented in Fig. 7. The first breaks were picked on a raw shot gather (Fig. 7a). After WET inversion of the first arrivals (Fig. 7c), surface static corrections were applied. The sudden time shift of the first breaks and of the bedrock reflection at an offset of approximately 35 m is clearly removed after these corrections (Fig. 7b). A super-gather that combines four CMP gathers and its semblance analysis are shown in Fig. 7d and e, respectively. Several reflections can be observed on the gather with clear semblance peaks. The velocity analysis includes velocities from reflections in black and velocities from refractions in green. The velocities from the refractions are necessary because no reflections can be seen before 60 ms. Finally, the NMO corrected gather is shown in Fig. 7f. For early times, the severe stretch mute is caused by the velocity variations in the first few meters.

Table 2

CMP processing of P-wave reflections. The steps identified by an asterisk were performed with in-house MATLAB codes based on the CREWES algorithms.

Processing step	Description
1. Surface static corrections*	Model used: 285, 547, and 1351 m/s with intersection times at 0, 3.8, and 9.8 ms, respectively
2. CMP binning	Bin length: 1.5 m
3. Bad trace removal*	Automatic based on S/N ratio
4. Scaling	AGC with a window of 250 ms
5. Predictive deconvolution	Lag: 5 ms. Window: 50 ms
6. Ormsby band-pass filter	60, 120, 650, and 800 Hz trapezoid frequencies
7. First break muting	
8. Semblance analysis	Includes the refraction model
9. NMO correction	Stretch mute: 75%
10. Alpha trim stacking	Alpha trim percentage: 75%
11. AGC	Window: 15 ms
12. Band-pass filter	60, 120, 650, and 800 Hz trapezoid frequencies
13. Median filter	Length: 5 traces
14. Depth conversion	f-k migration using the smoothed velocity model
15. Topographic shift	

6.1.5. Interpretation

The SV and P-wave time sections for the Buckingham case study are shown in Fig. 8, and the depth sections overlain by the velocity models are shown in Fig. 9. A very coherent reflection extends from 550 ms at the northern end (left side) to 850 ms at the southern end (right side) in the S-wave section (Fig. 8a) and from 75 to 125 ms in the P-wave section (Fig. 8b). When converted to depth (Fig. 9), this reflection deepens from 45 m at the northern end to 90 m in the middle of both sections to as deep as 120 m at the southern end. This is consistent with the depth to bedrock provided by boreholes in the area. This reflection is therefore interpreted as the bedrock contact. Every reflection below this reflection is a multiple. On the SV-wave stacked section, this interpretation is supported by the fact that the multiples have the same stacking velocity as the bedrock reflection. In the P-wave section, greater offsets would have been required to obtain a confident velocity estimate below the bedrock surface, so those reflections cannot be reliably interpreted; however, they are most likely multiples from the bedrock reflection. In both cases, a strong multiple from the bedrock is present at twice the traveltime of the primary and is visible for the first 400 m on both profiles. The presence of multiples for such deep reflections illustrates the depth of investigation that can be achieved using a simple sledgehammer source in this environmental setting.

Both sections also show a reflection along the survey line at times between 250 and 400 ms for S-waves and between 48 and 100 ms for P-waves (Fig. 8). On the depth sections (Fig. 9), this reflection is present at depths between 14 and 31 m and corresponds to the contact between the near surface clay unit and the sand and gravel unit. This confirms and clarifies the information found in nearby boreholes that was described above.

In the S-wave section, the clay–sand reflection is coherent between 0 and 500 m (see point 1 in Fig. 8). At distances greater than 500 m, the coherence is lost and the reflections appear to thicken (point 2). At least two factors may explain this loss of coherence. First, according to Aylsworth et al. (2000), the clay sediments over the bedrock at depths greater than 50 m were disturbed by a Holocene earthquake in the Outaouais region, which is prone to high seismicity. Pullan et al. (2011) attributed this loss of coherence to this earthquake event. Second, the presence of coarser material, such as a gravel deposit, can induce the scattering of the S-wave energy due to its small wavelength of approximately 2 m. Gravely layers over a finer mix of sand and gravel were encountered below the clay unit in several boreholes in the area.

Several reflections are present in the sand and gravel unit in the P-wave section that are not clearly present in the S-wave section (point 3 in Fig. 8b). This is the result of two phenomena. First, the stacking velocity for the reflections between the clay–sand interface and the bedrock reflections varies from 150 m/s to more than 250 m/s. This causes severe stretching after the NMO correction that had to be muted before stacking. As a result, a significant amount of the energy was removed, which resulted in poor signal-to-noise ratios for some reflections.

Second, some reflections are still present in the S-wave section, but they cannot be distinguished because of the higher impedance contrasts between the clay–sand and sand–bedrock contacts than the layering in the sand and gravel unit. With such large velocity variations, the density does not contribute significantly to the impedance contrast. For instance, the S-wave velocity varies from 150 m/s in the clay unit to more than 250 m/s in the sand and gravel unit. The reflections within the sand and gravel unit do not have sufficient energy to appear in the S-wave section with the gain settings that were used. They could be revealed using an AGC gain with a short window, but much of the amplitude information would be lost. On the other hand, the P-wave velocity difference between these units is much smaller and varies from 1500 m/s in the clay unit to approximately 1700 m/s in the sand and gravel unit. This makes the energy of the reflections more equal and they have similar amplitudes on the stacked section. The sections are then mutually complementary, and their combined interpretation

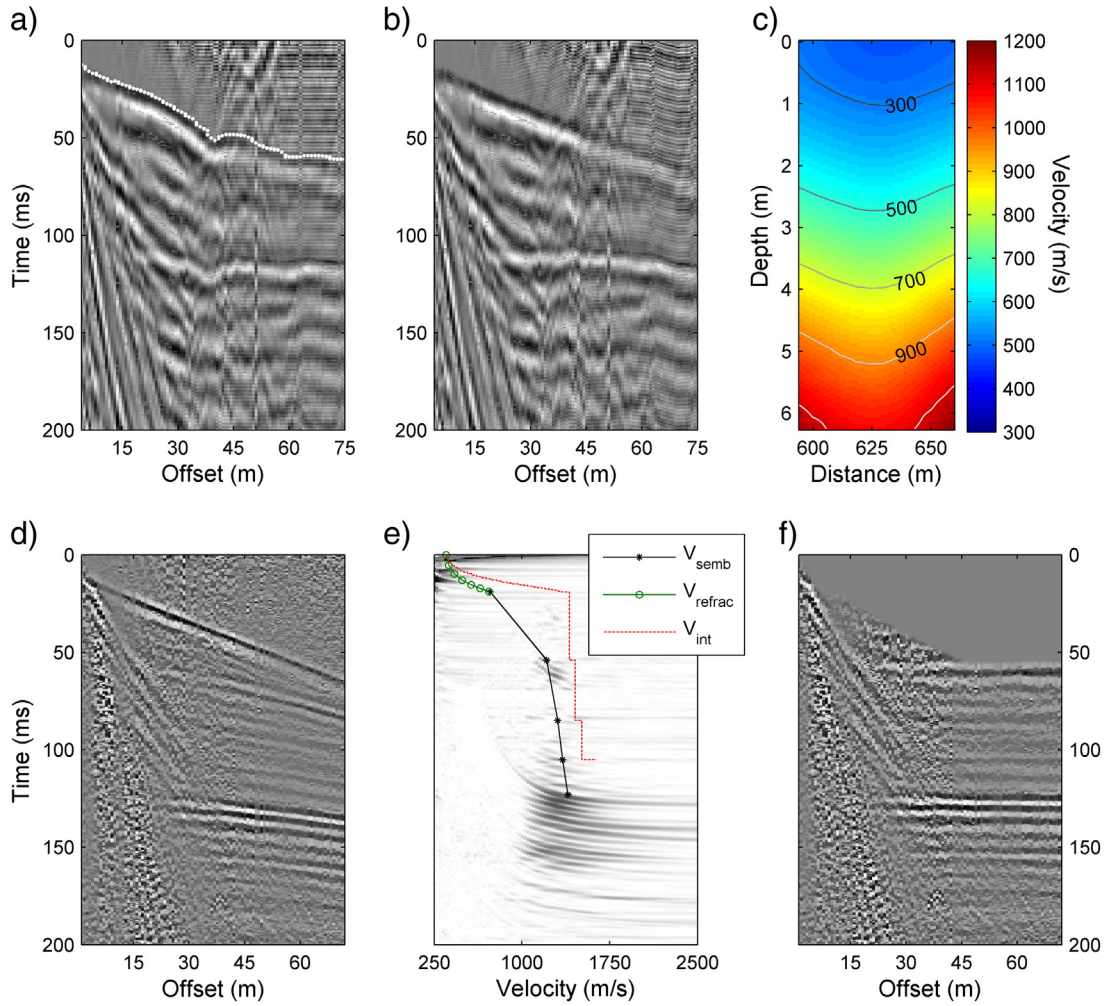


Fig. 7. An example of the processing of P-wave reflections: a) first breaks picked for shot gather no. 217 along the survey line of the Buckingham case study, b) the same shot gather after surface static corrections, c) P-wave velocity model obtained by WET inversion of the arrival times of the first breaks, d) CMP gather no. 772, e) semblance analysis of P-waves using the refraction results, and f) NMO-corrected CMP gather with a stretch mute of 75%.

provides a far better interpretative cross-section than by considering only one of these sections (Fig. 9c).

The P-wave section is blind within the first few meters of soil. However, the S-wave section provides great detail at shallow depths; in fact, many reflections are present in the shallow clay layer. For instance, parallel horizontal reflections are present in the clay unit (see point 4 in Fig. 8a) and are attributed to thin sand beds (Fabien-Ouellet et al., 2014). Dipping structures are also present (point 5 in Fig. 8a) and could be interpreted as landslide scars or ancient riverbeds.

Both the P- and SV-wave reflections are affected by strong statics due to topographic variations at distances of 500 and 1300 m along the survey line (points 6 and 7 in Fig. 8a). This was addressed by the static corrections for the P-wave section, but no easy solution was found for the S-wave section. The absence of static corrections for S-waves can be observed clearly at point 6 in Fig. 8a; a bump is present in the S-wave section that does not appear in the P-wave section. Without static corrections (not shown herein), the P-wave section would also exhibit this pattern due to the topography. The presence of statics must be taken into account during interpretation.

The combined velocity models (Fig. 9) are good interpretation tools. Because the S-wave velocities of unconsolidated sediments can vary by as much as four folds, this seismic property is very useful for distinguishing soft from hard materials. The difference in S-wave velocity between the clay unit (150 m/s) and the sand and gravel unit (200 to 350 m/s) is clear (Fig. 9a). The variation in P-wave velocity is much more subtle for the same units (Fig. 9b).

Because fluids do not sustain S-waves, soil saturation does not affect the S-wave velocity. However, the P-waves are very sensitive to water content and can indicate the depth to the capillary fringe. A change in P-wave velocity from 350 to 1500 m/s can occur in a clay deposit from unsaturated to fully saturated conditions. In the stacked P-wave section (Fig. 9b), no reflection can be associated with this abrupt impedance change because the water table is too shallow (approximately 6 m). This portion of the velocity model is obtained from the refraction analysis and shows the strength of combining refraction and reflection analyses.

In summary, the processing workflow used in this seismic survey was successful in characterizing a confined aquifer at depths as great as 90 m at a resolution on the order of 2 m (Fig. 9c). Only the seismic reflection method using SV-waves can achieve such results. This methodology leads to velocity models and stacked sections of SV-waves and P-waves, and provides much more information than the processing of P-waves alone. The combination of all of this information leads to a robust interpretation that confirms and clarifies the general interpretation provided by boreholes in the area.

6.2. Shawville case study: a survey over a silt deposit

To illustrate the performance of the FV-LMO filter, a short seismic survey over a silt deposit is presented. Although this filter was used for the Buckingham case study (compare Fig. 6d and a), the smaller length of the Shawville line makes the effects of the FV-LMO filter easier

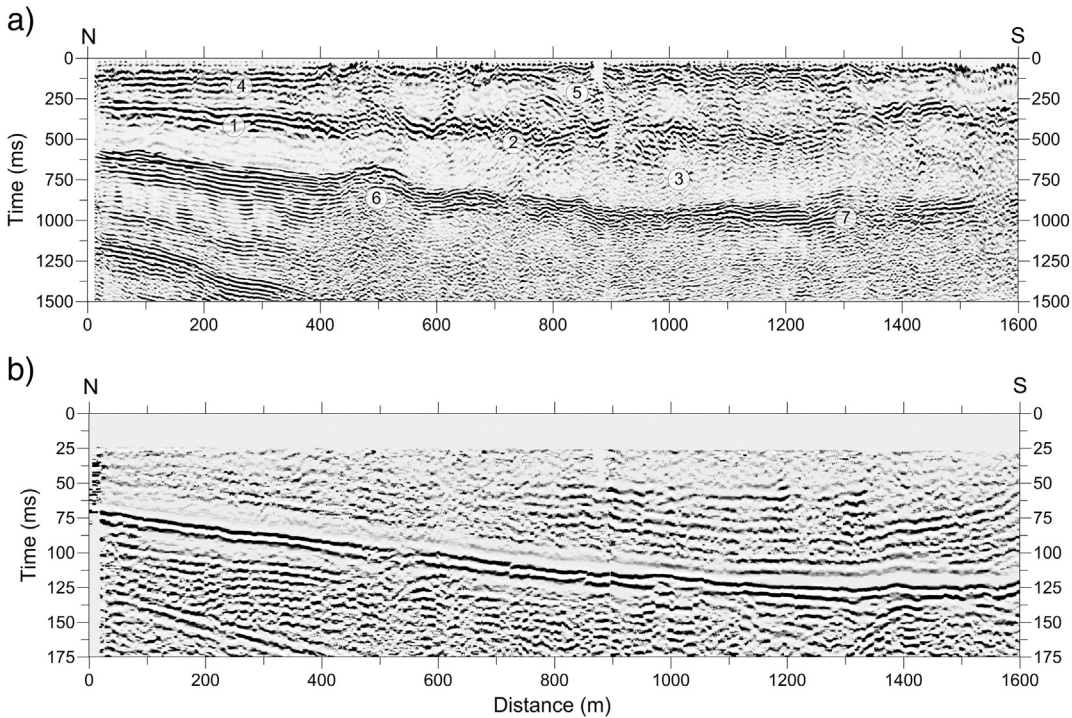


Fig. 8. a) SV-wave stacked section in time and b) P-wave stacked section in time for the Buckingham case study. The very coherent SV-wave reflections detected only with the vertical geophones are shown in this example.

to appraise. Along with other geophysical investigations, this seismic line was part of an effort to extend information laterally from a nearby piezocone penetration test (CPTu) (Fig. 3). The general objective was to build a hydrostratigraphic model to use for transport modeling. The acquisition parameters are the same as for the Buckingham survey except that each shot position was revisited only twice instead of four times due to the shallower bedrock.

The surface waves in the Shawville case study are very energetic (Fig. 10a). They hide some reflections and overlap the bedrock reflection at 300 ms. After the FV-LMO filtering (Fig. 10c), nearly of all the surface waves are gone, and new reflections appear, as shown by the blue arrows. In addition, a PS reflection that was nearly hidden by surface waves appears after applying the FV-LMO filter. In comparison, the application of a velocity fan reject filter in the f-k domain (Fig. 10b) leaves most of the surface wave energy intact.

The depth stacked sections for the Shawville survey are shown in Fig. 11. They were produced using a processing flow similar that in the first case study. On the SV-wave section after FV-LMO filtering (Fig. 11c), the bedrock reflection at a depth of approximately 25 m is more pronounced, the reflection at a depth of approximately 12.5 m is clearer and several near surface reflections appear much more clearly than on the SV-wave section after only pass-band filtering (Fig. 11a). Contamination by surface waves is evident in Fig. 11a; the stacking of the linear arrivals of surface waves causes the dipping features at depths less than 15 m. Fig. 11b shows the stacked section where the surface waves were muted by the top mute shown in Fig. 10a. All of the reflections above the bedrock are removed by the top mute because the surface waves and SV-reflections strongly overlap in this survey. Hence, muting is not appropriate in this case. Those results show the strength of the FV-LMO filter. More generally, this profile highlights the importance of filtering surface waves for SV-wave reflection processing; new features become apparent and false reflections are avoided.

Only the bedrock reflection appears in the P-wave stacked section (Fig. 11d). The discontinuity of the bedrock reflection at a distance of 50 m in the SV-wave section also appears in the P-wave section but is smoothed due to the longer wavelength of the P-waves. Early

SV-wave reflections are confirmed by the CPTu that was carried out a few meters away from the survey line. According to the CPTu logs (Fig. 11e), a superficial 5 m thick sandy silt layer overlies a deep clayey silt unit. At depths greater than 13 m, the friction ratio becomes noisier, indicating the presence of a sandier clay deposit. This correlates very well with the seismic section, on which two main reflections appear above the bedrock: one at a depth of 5.3 m at the contact between the sandy silt unit and the clayey silt unit and the other at a depth of 12.5 m due to traces of fine sand. Penetration refusal on bedrock occurred at a depth of 30 m, which is consistent with the seismic sections. The results of the seismic survey confirm the lateral extension of the units obtained from the CPTu interpretation; therefore this information can be extended spatially along the line.

6.3. Lake Green case study: a survey over a sand deposit

To highlight the fact that vertical geophones cannot be used in all conditions for the acquisition of SV-wave reflections, a seismic survey over a sand deposit is presented in the last case study. The same acquisition parameters that were used in the Buckingham case study were used for this survey. A shot gather is shown in Fig. 12. No SV-wave reflections appear in this shot gather, and only back-scattered surface wave patterns are present where SV-wave reflections should be found. Moreover, surface waves are also difficult to distinguish because other arrivals are superposed over them. To determine if reflections are hidden by Rayleigh waves, the shot gather in Fig. 12a was processed using the FV-LMO filter applied in both directions to remove back-scattered surface waves (Fig. 12c). Using the MASW velocity model and the depth to bedrock obtained by processing the P-wave reflections, the expected SV-wave reflections were calculated using the NMO equation. This region is shaded in red in Fig. 12c. There is still no coherent reflection because the particle motion is more or less horizontal in this survey. This is supported by the velocity profile found from the inversion of the fundamental mode of the Rayleigh waves (inset in Fig. 12b). There is no S-wave velocity inversion, and the S-wave velocities increase regularly with depth from 200 m/s to more than 300 m/s in the first 8 m of the sand deposit. In such conditions,

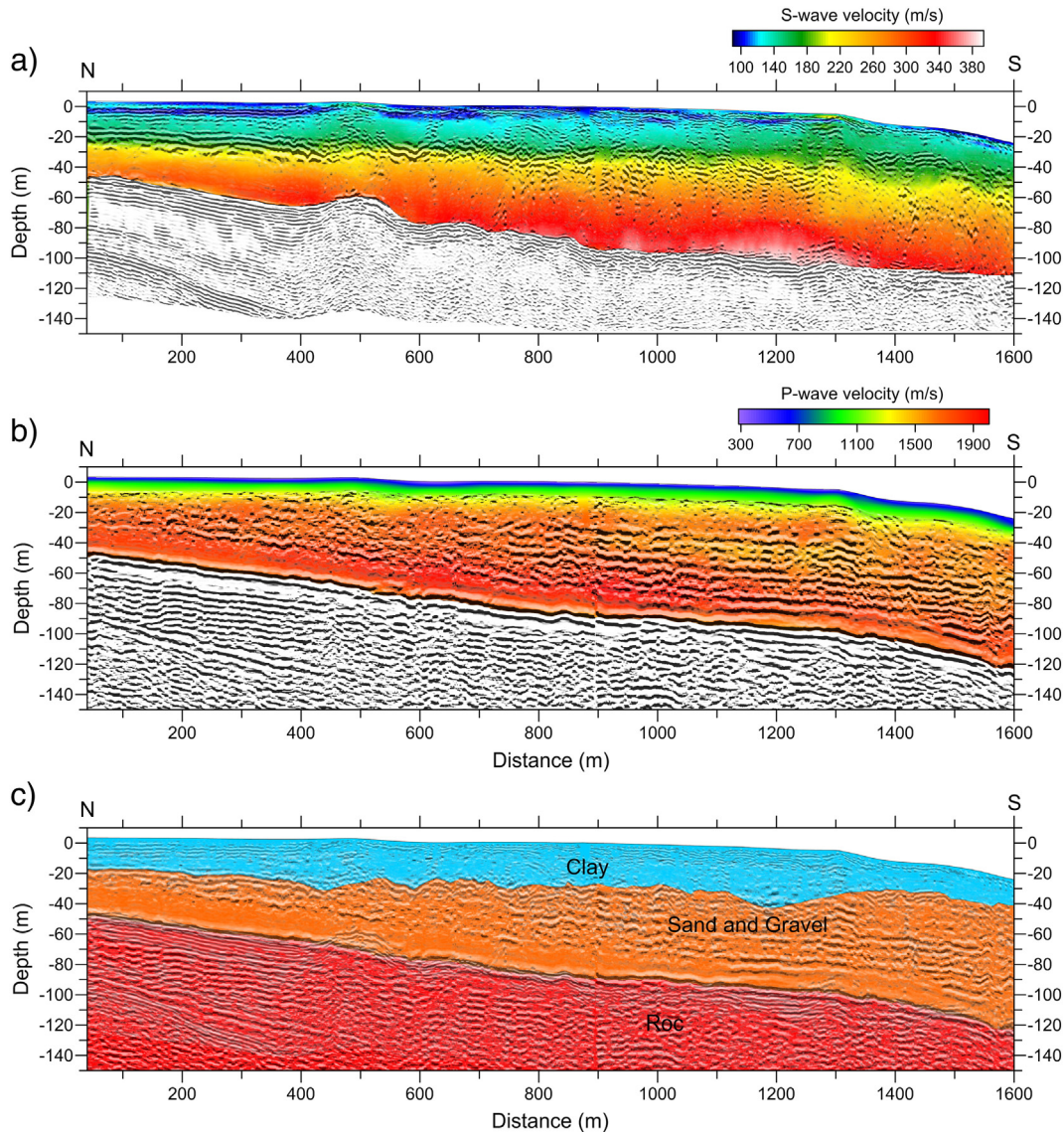


Fig. 9. Stacked sections in depth overlaid by the combined velocity model for the Buckingham case study: a) SV-wave section and b) P-wave section. c) Hydrostratigraphic interpretation overlaid by both P- and SV-wave sections.

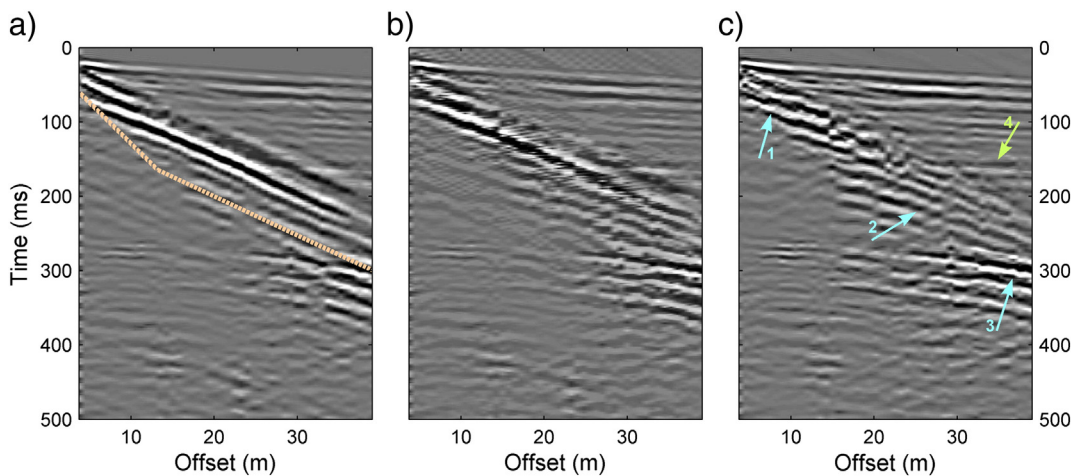


Fig. 10. Shot gather no. 3 along the Shawville survey line: a) without filtering; the top mute used in Fig. 11b is indicated by the orange dashed line, b) f-k filtering for velocities between 130 and 250 m/s, and c) FV-LMO filtering as proposed by Park et al. (2002b), which allows a better identification of the reflections than without filtering; the blue arrows (nos. 1, 2 and 3) show SV-wave reflections, and the green arrow (no. 4) shows PS-wave reflections.

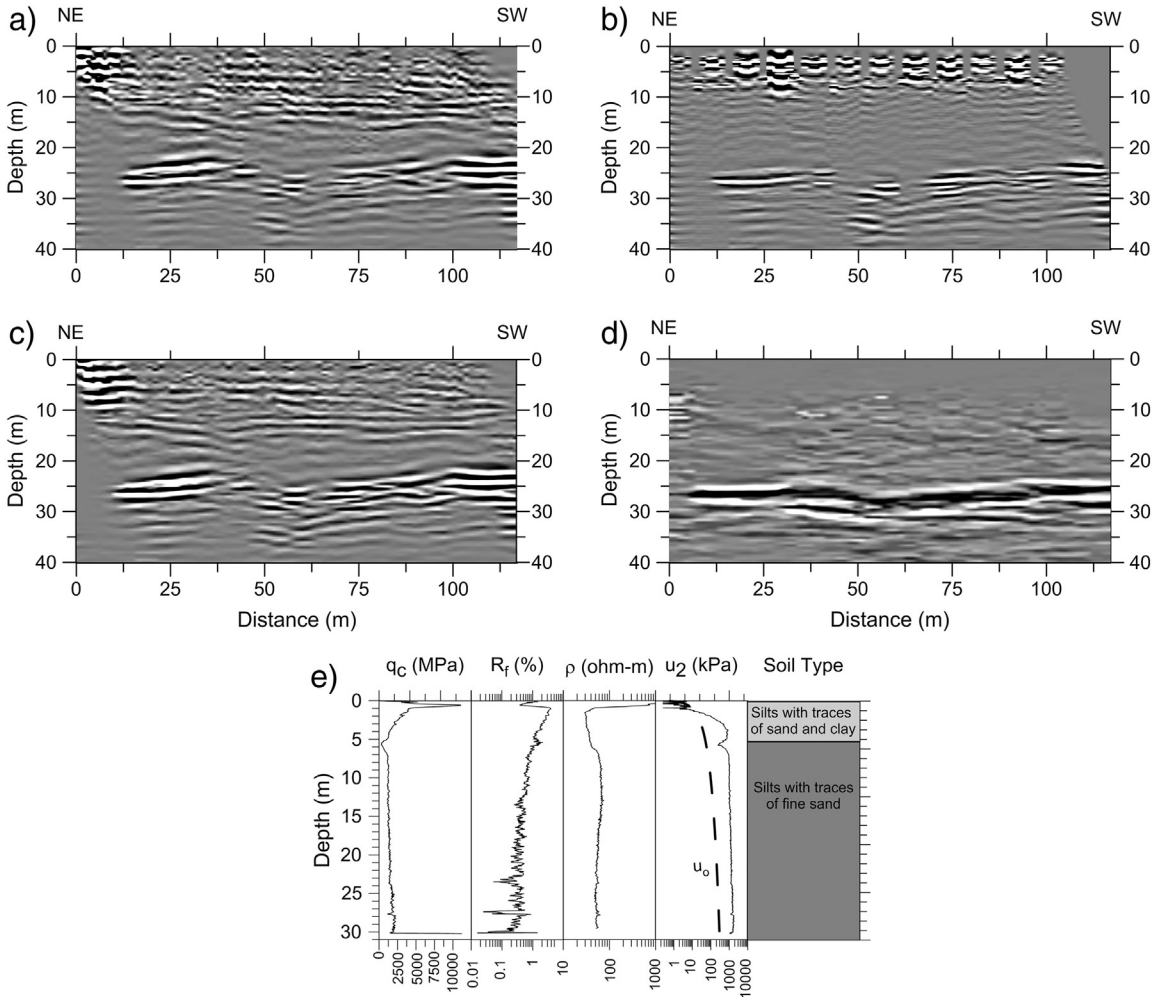


Fig. 11. Depth stacked sections for the Shawville case study: a) SV-wave section after an Ormsby band-pass filter with corner frequencies of 30, 50, 200, and 300 Hz, b) SV-wave section obtained by muting the surface waves, c) SV-wave section after FV-LMO filtering, and d) P-wave section. e) Results from a piezocone penetration test performed close to the survey line; q_c is the cone resistance, R_f is the friction ratio, ρ is the electrical resistivity, and u_2 is the pore pressure. Modified from Comeau et al. (2012).

the seismic ray paths at the surface are almost vertical for short offsets and the particle motion due to the propagation of S-waves is in the horizontal plane. Thus, in contrast to the Buckingham and Shawville case studies over clay and silt deposits, horizontal geophones would have been necessary to record S-wave reflections in the Lake Green survey.

Even though SV-wave reflections were not recorded in the Lake Green survey, the proposed workflow can still be used. As described in the previous paragraph, MASW can be performed. This leads to an SV-wave velocity model (Fig. 12b) that provides the shear wave velocity for shallow depths. Filtering surface waves is helpful to assess the

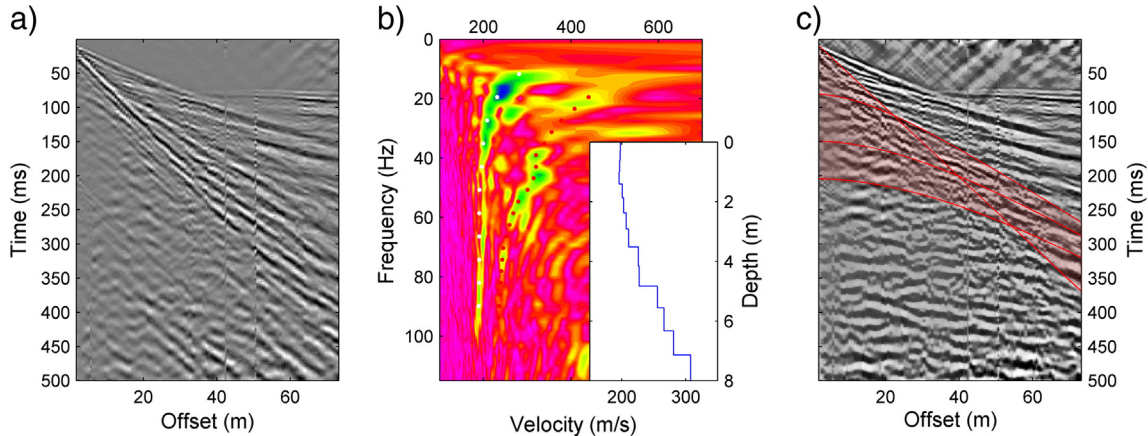


Fig. 12. A shot gather along the survey line of the Lake Green case study: a) without filtering, b) dispersion analysis of surface waves, where the fundamental mode is identified by white dots, and the superior modes are identified by the red dots (the inset shows the velocity model obtained by the inversion of the fundamental mode), and c) the filtered shot gather, overlaid by the expected SV-wave reflections. (For interpretation of the references to color in this figure legend, the reader is referred to the web version of this article.)

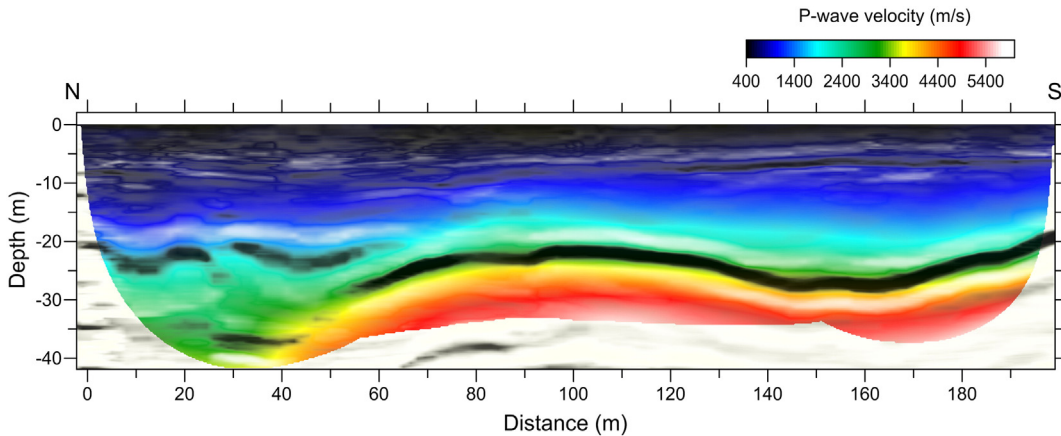


Fig. 13. Seismic refraction P-wave velocity model overlaid by the P-wave stacked section for the Lake Green survey.

presence or absence of SV-reflections and provides a better understanding of the seismic data. Seismic refraction tomography and P-wave seismic reflection were also possible with this dataset (Fig. 13). This figure shows the very good fit between both methods. Three main reflections are present in this section. The shallowest reflection is interpreted as the water table because the P-wave velocity increases from 500 to 1500 m/s at this interface. This is very consistent with the water level of Lake Green, which is located 50 m north of the line. At the northern end of the profile, an intermediate reflection is created by a unit with a mean velocity of 2000 m/s. This is consistent with a till deposit. The last reflection corresponds to bedrock with a mean velocity of 5000 m/s.

7. Conclusions

The conversion between SV- and P-waves at interfaces produces a more complex system than SH-waves. For this reason, most research has focused on SH-waves (Helbig and Mesdag, 1982). However, this complexity can be used to increase the value of the survey because information can be obtained from many seismic arrivals, including Rayleigh waves, first arrivals, and P-wave, SV-wave and PS-wave reflections. In contrast to SH-waves, no special sources are required to generate SV-waves; a simple sledgehammer is sufficient.

In general, vertical and horizontal geophones (2-C) are required to perform an SV-wave reflection survey. However, in some cases, SV-wave reflections can be recorded by vertical geophones, as shown in this study. For this reason, the presence of SV-wave reflections should be evaluated during data processing even if only vertical geophones are used. In a general seismic survey that is not designed for SV-wave acquisition, small geophone spacings and long record lengths should be used to maximize the chances of detecting SV-waves and successfully processing them.

The processing of SV-wave reflections can be more complex and time consuming than P-wave reflections due to their high sensitivity to the stacking velocity. A careful velocity analysis must be performed because small errors in stacking velocity can lead to a severe loss of coherence in the stacked section. However, the processing of Rayleigh waves with MASW can help to obtain a suitable velocity model.

Surface waves interference during stacking can also be problematic. The FV-LMO filter is much more efficient at removing surface waves than a simple f-k filter. Surface waves should not be considered noise. On the contrary, their processing can be helpful during SV-wave reflection processing as long as the reflections contain sufficient energy. Furthermore, Rayleigh waves are generally produced in all seismic surveys and can be used to estimate the variation in SV-wave velocity in the first few meters of soil.

Finally, the proposed combined workflow is only a first step in using all of the information contained in the P-SV system. A more rigorous method has to be developed as a single inversion scheme for all seismic

arrivals. This could be achieved by full waveform inversion based on the elastic wave equation. However, the proposed workflow has the advantage of being based on readily available inversion algorithms and can be implemented at low cost.

Acknowledgments

Funding for this research came in part from the *Ministère du développement durable, de l'environnement, de la faune et des parcs* (MDDEFP) of the province of Québec, Canada, the Natural Sciences and Engineering Research Council (NSERC) of Canada and from the *Fonds de recherche du Québec - Nature et technologies*. We also thank Simon Bérubé, Majid El Baroudi, Yan Vincent and Alexandra Roberge for their help in the field. We acknowledge the helpful advice of Christian Dupuis in writing and editing the paper.

References

- Aki, K., Richards, P.G., 2002. *Quantitative Seismology* 2nd edition. Univ Science Books.
- Leduc, E., Daigneault, R.A., Roy, M., et Lamothe, M., 2013. Géologie des formations superficielles de la région de Cobden (31 F10); carte présentée au Ministère des Ressources Naturelles du Québec, scale 1:50000.
- Hurtubise, M.A., Milette, S., Daigneault, R.A., Roy, M. et Lamothe M., 2012. Géologie des formations superficielles de la région de Thuro (31G11); carte présentée au Ministère des ressources naturelles et de la Faune du Québec, scale 1:50 000.
- Aylsworth, J.M., Lawrence, D.E., Guertin, J., 2000. Did two massive earthquakes in the Holocene induce widespread landsliding and near-surface deformation in part of the Ottawa Valley, Canada? *Geology* 28 (10), 903–906. [http://dx.doi.org/10.1130/0091-7613\(2000\)28<903:DTMEIT>2.0.CO;2](http://dx.doi.org/10.1130/0091-7613(2000)28<903:DTMEIT>2.0.CO;2).
- Comeau, G., Molson, J., Lemieux, J.M., Talbot, M.C., Therrien, R., Montcouidiol, N., Ayotte, S., Bérubé, S., Fabien-Ouellet, G., Fiset, P., Fortier, R., Graf, T., Moreno, A., Sterckx, A., 2012. Projet d'acquisition de connaissances sur les eaux souterraines en Outaouais, Rapport d'étape II. Département de géologie et de génie géologique, Université Laval 54 (mars 2012).
- Fabien-Ouellet, G., Fortier, R., Giroux, B., 2014. Joint acquisition and processing of seismic reflections and surface waves in a sensitive clay deposit in the Outaouais Region (Québec), Canada. *Landslides in Sensitive Clays*. Springer Netherlands, pp. 241–252. http://dx.doi.org/10.1007/978-94-007-7079-9_19_0.
- Guy, E.D., Nolen-Hoeksema, R.C., Daniels, J.J., Lefchik, T., 2003. High-resolution SH-wave seismic reflection investigations near a coal mine-related roadway collapse feature. *J. Appl. Geophys.* 54 (1), 51–70. [http://dx.doi.org/10.1016/S0926-9851\(03\)00055-7](http://dx.doi.org/10.1016/S0926-9851(03)00055-7).
- Hagedoorn, J.G., 1959. The plus-minus method of interpreting seismic refraction sections. *Geophys. Prospect.* 7 (2), 158–182. <http://dx.doi.org/10.1111/j.1365-2478.1959.tb01460.x>.
- Haines, S.S., Ellefsen, K.J., 2010. Shear-wave seismic reflection studies of unconsolidated sediments in the near surface. *Geophysics* 75 (2), B59–B66. <http://dx.doi.org/10.1190/1.3340969>.
- Helbig, K., Mesdag, C.S., 1982. The potential of shear wave observations. *Geophys. Prospect.* 30 (4), 413–431. <http://dx.doi.org/10.1111/j.1365-2478.1982.tb01314.x>.
- Hunter, J.A., Benjumea, B., Harris, J.B., Miller, R.D., Pullan, S.E., Burns, R.A., Good, R.L., 2002. Surface and downhole shear wave seismic methods for thick soil site investigations. *Soil Dyn. Earthq. Eng.* 22 (9), 931–941. [http://dx.doi.org/10.1016/S0267-7261\(02\)00117-3](http://dx.doi.org/10.1016/S0267-7261(02)00117-3).
- Lai, C.G., Rix, G.J., 1998. Simultaneous inversion of Rayleigh phase velocity and attenuation for near-surface site characterization. School of Civil and Environmental Engineering, Georgia Institute of Technology 258.

- Lai, C.G., Rix, G.J., Foti, S., Roma, V., 2002. Simultaneous measurement and inversion of surface wave dispersion and attenuation curves. *Soil Dyn. Earthq. Eng.* 22 (9), 923–930. [http://dx.doi.org/10.1016/S0267-7261\(02\)00116-1](http://dx.doi.org/10.1016/S0267-7261(02)00116-1).
- Lanz, E., Maurer, H., Green, A.G., 1998. Refraction tomography over a buried waste disposal site. *Geophysics* 63 (4), 1414–1433. <http://dx.doi.org/10.1190/1.1444443>.
- Margrave, G.F., 2003. *Numerical Methods of Exploration Seismology with Algorithms in MATLAB*. Department of Geology and Geophysics, University of Calgary (225 pp.).
- Motazedian, D., Hunter, J.A., 2008. Development of an NEHRP map for the Orleans suburb of Ottawa, Ontario. *Can. Geotech. J.* 45 (8), 1180–1188. <http://dx.doi.org/10.1139/T08-051>.
- O'Neill, A., Dentith, M., List, R., 2003. Full-waveform P-SV reflectivity inversion of surface waves for shallow engineering applications. *Explor. Geophys.* 34 (3), 158–173. <http://dx.doi.org/10.1071/EG03158>.
- Palmer, D., 1981. An introduction to the generalized reciprocal method of seismic refraction interpretation. *Geophysics* 46 (11), 1508–1518. <http://dx.doi.org/10.1190/1.1441157>.
- Park, C.B., Miller, R.D., Xia, J., 1998. Imaging dispersion curves of surface waves on multi-channel record. *SEG Expand. Abstr.* 17 (1), 1377–1380. <http://dx.doi.org/10.1190/1.1820161>.
- Park, C.B., Miller, R.D., Xia, J., 1999. Multichannel analysis of surface waves. *Geophysics* 64 (3), 800–808. <http://dx.doi.org/10.1190/1.1444590>.
- Park, C.B., Miller, R.D., Ivanov, J., 2002a. Filtering surface waves. *Symposium on the Application of Geophysics to Engineering and Environmental Problems 2002*. Society of Exploration Geophysicists SEI9-SEI9.
- Park, C.B., Miller, R.D., Miura, H., 2002b. Optimum field parameters of an MASW survey. *Exp. Abs. SEG-J Tokyo* 22–23 (17–18 May).
- Pugin, A., Pullan, S.E., 2000. First-arrival alignment static corrections applied to shallow seismic reflection data. *J. Environ. Eng. Geophys.* 5 (1), 7–15.
- Pugin, A.J.M., Larson, T.H., Sargent, S.L., McBride, J.H., Bexfield, C.E., 2004. Near-surface mapping using SH-wave and P-wave seismic land-streamer data acquisition in Illinois, US. *Lead. Edge* 23 (7), 677–682. <http://dx.doi.org/10.1190/1.1776740>.
- Pugin, A.J.M., Pullan, S.E., Hunter, J.A., 2008. SV-wave and P-wave high resolution seismic reflection using vertical impacting and vibrating sources. 21st EEGS Symposium on the Application of Geophysics to Engineering and Environmental Problems.
- Pugin, A.J.M., Pullan, S.E., Hunter, J.A., 2009. Multicomponent high-resolution seismic reflection profiling. *Lead. Edge* 28 (10), 1248–1261. <http://dx.doi.org/10.1190/1.3249782>.
- Pugin, A.J.M., Brewer, K., Cartwright, T., Pullan, S.E., Perret, D., Crow, H., Hunter, J.A., 2013. Near surface S-wave seismic reflection profiling – new approaches and insights. *First Break* 31 (3), 49–60. <http://dx.doi.org/10.3997/1365-2397.2013005> (February 2013).
- Pullan, S.E., Pugin, A.J.M., Hunter, J.A., Brooks, G.R., 2011. Mapping disturbed ground using compressional and shear wave reflection sections. *Symposium on the Application of Geophysics to Engineering and Environmental Problems 2011*.
- Schuster, G.T., Quintus-Bosz, A., 1993. Wavepath eikonal traveltime inversion. *Theory. Geophys.* 58 (9), 1314–1323. <http://dx.doi.org/10.1190/1.1443514>.
- Sheehan, J.R., Doll, W.E., Mandell, W.A., 2005. An evaluation of methods and available software for seismic refraction tomography analysis. *J. Environ. Eng. Geophys.* 10 (1), 21–34. <http://dx.doi.org/10.2113/JEEG10.1.21>.
- Steeple, D.W., Miller, R.D., 1998. Avoiding pitfalls in shallow seismic reflection surveys. *Geophysics* 63 (4), 1213–1224. <http://dx.doi.org/10.1190/1.1444422>.
- White, D.J., 1989. Two-dimensional seismic refraction tomography. *Geophys. J. Int.* 97 (2), 223–245. <http://dx.doi.org/10.1111/j.1365-246X.1989.tb00498.x>.
- Xia, J., Miller, R.D., Park, C.B., 2000. Advantages of calculating shear-wave velocity from surface waves with higher modes. *Proceedings of the 70th Annual International Meeting, SEG, Expanded Abstracts*, pp. 1295–1298. <http://dx.doi.org/10.1190/1.1815633>.
- Xia, J., Miller, R.D., Park, C.B., Hunter, J.A., Harris, J.B., Ivanov, J., 2002. Comparing shear-wave velocity profiles inverted from multichannel surface wave with borehole measurements. *Soil Dyn. Earthq. Eng.* 22 (3), 181–190. [http://dx.doi.org/10.1016/S0267-7261\(02\)00008-8](http://dx.doi.org/10.1016/S0267-7261(02)00008-8).
- Xia, J., Miller, R.D., Park, C.B., Tian, G., 2003. Inversion of high frequency surface waves with fundamental and higher modes. *J. Appl. Geophys.* 52 (1), 45–57. [http://dx.doi.org/10.1016/S0926-9851\(02\)00239-2](http://dx.doi.org/10.1016/S0926-9851(02)00239-2).
- Xia, J., Xu, Y., Miller, R.D., Ivanov, J., 2012. Estimation of near-surface quality factors by constrained inversion of Rayleigh-wave attenuation coefficients. *J. Appl. Geophys.* 82 (2012), 137–144. <http://dx.doi.org/10.1016/j.jappgeo.2012.03.003>.
- Zhang, J., Toksöz, M.N., 1998. Nonlinear refraction traveltime tomography. *Geophysics* 63 (5), 1726–1737. <http://dx.doi.org/10.1190/1.1444468>.